Prediction of Dissolved Oxygen and Carbon Dioxide Concentration Profiles in Tubular Photobioreactors for Microalgal Culture

F. Camacho Rubio,[1] F. G. Acién Fernández,[2] J. A. Sánchez Pérez,[2] F. García Camacho,[2] E. Molina Grima[2]

[1]Department of Chemical Engineering, University of Granada, Granada, Spain
[2]Department of Chemical Engineering, University of Almería, E-04071 Almería Spain; telephone: +34 50 215032; fax: +34 50 215070; e-mail: emolina@ualm.es

Received 18 March 1998; accepted 24 June 1998

Abstract: A model is developed for prediction of axial concentration profiles of dissolved oxygen and carbon dioxide in tubular photobioreactors used for culturing microalgae. Experimental data are used to verify the model for continuous outdoor culture of *Porphyridium cruentum* grown in a 200-L reactor with 100-m long tubular solar receiver. The culture was carried out at a dilution rate of 0.05 h^{-1} applied only during a 10-h daylight period. The quasi-steady state biomass concentration achieved was 3.0 $g \cdot L^{-1}$, corresponding to a biomass productivity of 1.5 $g \cdot L^{-1} \cdot d^{-1}$. The model could predict the dissolved oxygen level in both gas disengagement zone of the reactor and at the end of the loop, the exhaust gas composition, the amount of carbon dioxide injected, and the pH of the culture at each hour. In predicting the various parameters, the model took into account the length of the solar receiver tube, the rate of photosynthesis, the velocity of flow, the degree of mixing, and gas-liquid mass transfer. Because the model simulated the system behavior as a function of tube length and operational variables (superficial gas velocity in the riser, composition of carbon dioxide in the gas injected in the solar receiver and its injection rate), it could potentially be applied to rational design and scale-up of photobioreactors. *Biotechnol Bioeng* **62**: 71–86, 1999.
Keywords: photobioreactor; airlift bioreactor; microalgae; mass transfer; liquid circulation

INTRODUCTION

Microalgae have been traditionally cultivated in open systems where culture environment is selected to favor algal growth relative to that of contaminating microorganisms. Open systems permit little control, and a certain level of contamination always occurs. Moreover, open systems cannot be used with algae that, for optimal productivity, must be cultured under conditions that would allow proliferation of other potentially contaminating microbes. Production of high-value algal products from strains that cannot be maintained in open ponds requires closed systems such as tubular photobioreactors. One such design employs an airlift device for low-shear propulsion of culture fluid through a horizontal tubular loop that constitutes the solar receiver (Borowitzka, 1996; Gudin and Chaumont, 1983; Gudin and Therpenier, 1986; Lee, 1986; Molina Grima et al., 1994; Richmond et al., 1993; Torzillo et al., 1993; Tredici and Materassi, 1992). One end of the solar receiver tube is connected to the gas-injected riser of the airlift drive, and the other end is connected to the downcomer. The solar receiver tubes are usually thermostated for optimal biomass productivity. The liquid velocity, and hence, the flow regime, are controlled by regulating the air supply to the riser section of the airlift. The pH of the culture, and thus, the carbon availability are usually controlled by injecting pure carbon dioxide, whereas the average irradiance within the culture can be adjusted by modulating the dilution rate to control the light attenuation by the biomass (Acién Fernández et al., 1997, 1998; Molina Grima et al., 1996). Besides these factors, the culture yield is also influenced by the mass-transfer capacity of the reactor (Livansky et al., 1987, 1990, 1992; Talbot et al., 1991; Tsoglin et al., 1996).

Photosynthetic production of algae is always accompanied by evolution of oxygen and consumption of carbon dioxide. Oxygen levels above air saturation (0.2247 mol O_2 m^{-3} at 20°C) could inhibit photosynthesis in many algal species, even if carbon dioxide concentration is maintained at elevated levels (Aiba, 1982). In addition, elevated levels of oxygen combined with high levels of irradiance, can lead to severe photo-oxidation (Richmond, 1991). Therefore, an important aspect of design and scale-up of tubular photobioreactors is establishing combinations of tube length, flow rate, and irradiance levels that do not allow oxygen build-up to inhibitory levels.

While the practical feasibility of tubular reactors for microalgal culture has already been established, systematic

Correspondence to: E. Molina Grima

 CCC 0006-3592/99/010071-16

studies of these devices have only just begun. In the first detailed study of tubular reactors, Pirt et al. (1983) disregarded the oxygen accumulation problem. That work became the basis upon which an industrial culture facility was built by Photobioreactors Ltd in Cartagena, Spain. However, the operation failed, principally because a great proportion of the tube length was unproductive due to oxygen inhibition. Another important issue is that of carbon dioxide supply. Carbon constitutes about 50% of the algal biomass and the local carbon dioxide concentration at any point in the tube should not fall below a critical value, or the availability of the carbon source will limit photosynthesis. In principle, CO_2 limitation can be easily avoided by supplying it in excess, but use of carbon dioxide represents a major operational expense of microalgal culture; hence, loss of residual CO_2 in the exhaust gas needs to be minimized. Weissman et al. (1988) reported that CO_2 concentration in bulk liquid of at least 65 μM and pH 8.5 were required for optimal productivity of some marine- and saline-water diatoms. Similarly, Märkl and Mather (1985) observed a low critical CO_2 for *Chlorella vulgaris:* Concentrations as low as 60 μM enabled unlimited photosynthesis. In this regard, Lee and Hing (1989) have suggested supplying carbon dioxide by diffusion through silicone tubes containing the pure gas. In theory, this strategy can reduce CO_2 losses in the exhaust gas, but losses cannot be eliminated as Lee and Hing (1989) contend. Furthermore, the gas phase inside the tube would need to be purged from time to time because of dilution by counter-diffusion of oxygen. Lee and Hing (1989) also disregarded this. In practice, ensuring sufficiency of carbon source in a long, tubular bioreactor and simultaneous minimization of losses requires multiple gas injection points along the length of the tube. How far apart the injection points are spaced depends on several factors including the flow velocity of the liquid, the rate of photosynthesis (i.e., light intensity), the gas-liquid mass transfer coefficient, and the rate of carbon dioxide injection.

Although efficient management of the supply of carbon source is important, oxygen build-up is generally one of the greatest constraints for scale-up of tubular photobioreactors (Märkl and Mather, 1985; Richmond, 1990; Torzillo et al., 1986). In studies with *C. vulgaris*, Märkl and Mather (1985) noted that the rate of photosynthesis increased by 14% when there was almost no dissolved oxygen. Saturation of the medium with pure oxygen (i.e., a dissolved oxygen concentration of 1.38 mol O_2 m^{-3} at 20°C) reduced the photosynthesis rate by 35%. In practice, the minimum feasible level of dissolved oxygen is 21% of air saturation, because the nutrient feed tends to be in equilibrium with the atmosphere and air is used to drive the culture via the airlift pump.

Improved productivity of microalgal cultures in tubular photobioreactors demands a quantitative understanding of how the performance is affected by design and operational factors such as the length and tube diameter, the flow rate, the dissolved oxygen and carbon dioxide concentration profiles, and gas-liquid mass transfer. Also, in airlift-driven tubular systems a further consideration is the relationship between the induced liquid circulation rate in the tube and the gas-injection rate in the airlift section. The present work considers some of the issues noted here in developing a mechanistic model of airlift-driven tubular photobioreactors. The predictive capabilities of the model are demonstrated during outdoor continuous culture of the microalga *Porphyridium cruentum* that is potentially useful for producing certain polysaccharides and polyunsaturated fatty acids of therapeutic significance.

THE BIOREACTOR MODEL

A microalgal culture is a pseudohomogeneous gas-liquid two-phase system. The carbon dioxide gas injected is transported from the gas phase to the aqueous medium to provide the inorganic carbon and control the pH of the culture. For otherwise fixed conditions, the inorganic carbon supplied is incorporated into the cells at a specific rate determined by the rate of photosynthesis (Colman and Rotatore, 1995; Rados et al., 1975; Rotatore et al., 1995). Similarly, the oxygen is produced at a specific rate, and it transfers from the culture to the gas phase. Therefore, modeling of the reactor must consider gas-liquid mass transfer and the hydrodynamics (gas holdup, gas-liquid interfacial area) in the riser, the degasser, and the solar receiver loop. Whereas the dissolved oxygen and the inorganic carbon concentrations are strictly functions of time and position along the reactor, the model will assume only positional variations in a given short-time interval, i.e., the concentrations will be discretized in constant time intervals. This is reasonable because over a short-time increment during the early morning, midday, afternoon, or night, the rate of photosynthesis (the only time-dependent variable) varies only slowly; hence, within a given time increment, Δt, a mean value of the rate can be used for the entire increment. Furthermore, the model will assume that plug flow prevails in solar receiver tube and in most of the airlift zone, except the degasser where stirred tank behaviour will be assumed. These assumptions are well supported for flow in airlift devices (Ho et al., 1977; Fraser et al., 1994; Merchuk and Siegel, 1988;) and in pipes; nonetheless, direct evidence for the assumed flow behavior will be presented later for a photobioreactor geometrically similar to the one used for the culture.

Combining Flow and Gas-Liquid Mass Transfer

Because of the very small gas holdup and the small diameter of bubbles in the horizontal solar loop, a homogeneous flow situation (i.e., no slip between phases) will be assumed in this zone. Furthermore, at any hydrodynamic steady state, the volumetric flow rate Q_L of the liquid phase is assumed to remain constant. Because of photosynthesis in the liquid phase, carbon dioxide is being consumed and oxygen is being produced. These changes in composition of the liquid phase give rise to a continuous exchange of the oxygen and carbon dioxide between the gas and the liquid phases (Fig. 1). Because only carbon dioxide is injected into the solar

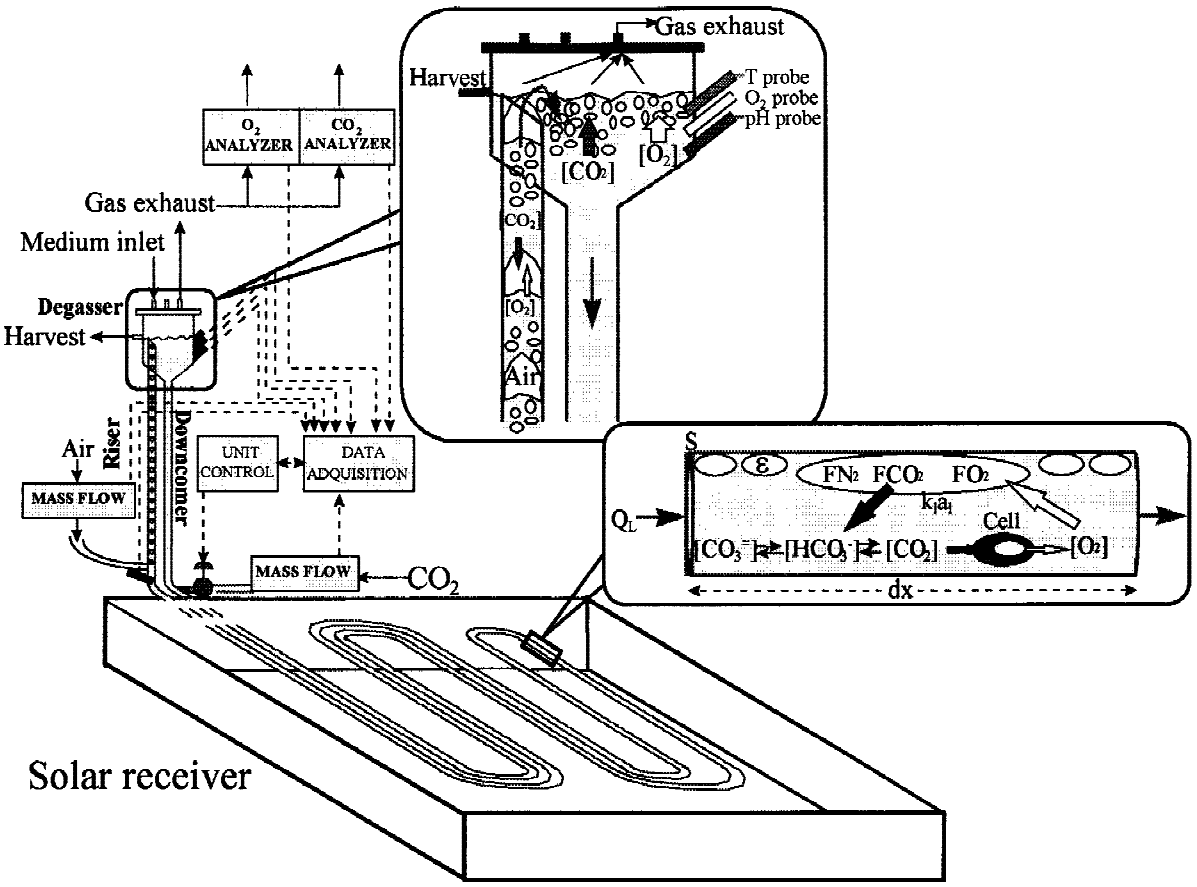

Figure 1. Schematic drawing of the tubular photobioreactor used, showing the nomenclature and phenomena taking place in the system (solar receiver 98.8 m).

loop, the gas phase is made exclusively of CO_2 and photosynthetically generated oxygen (although some nitrogen also transfers to the gas phase because the culture entering the solar loop is saturated with air). In addition, the gas phase is assumed to be saturated with water at the isothermal conditions of the culture.

For the liquid phase in plug flow, the changes in concentrations of dissolved oxygen and dissolved inorganic carbon along the loop can be related to the gas-liquid mass transfer rates and the generation/consumption rates by mass balances as follows:

$$Q_L\, d[O_2] = K_1 a_{11_{O_2}}([O_2]^* - [O_2])Sdx + R_{O_2}(1-\varepsilon_1)Sdx \qquad (1)$$

$$Q_L\, d[C_T] = K_1 a_{11_{CO_2}}([CO_2]^* - [CO_2])Sdx + R_{CO_2}(1-\varepsilon_1)Sdx \qquad (2)$$

In these equations, $K_{lal\ 1\ O2}$ and $K_{lal\ 1\ CO2}$ are the volumetric gas-liquid mass transfer coefficient for oxygen and carbon dioxide, respectively; dx is the differential distance along the direction of flow in the solar tube; $[O_2]$, $[C_T]$ and $[CO_2]$ are the liquid phase concentrations of oxygen, inorganic carbon, and carbon dioxide, respectively; ϵ_1 is the gas holdup; S is the cross-sectional area of the tube; R_{O2} and R_{CO2} are the volumetric generation and consumption rate of oxygen and carbon dioxide, respectively; and Q_L is the volumetric flow rate of the liquid. Note that the concentration values marked with asterisks are equilibrium concentrations, i.e., the maximum possible liquid-phase concentration of the component in contact with the gas phase of a given composition. In eqs. (1) and (2), the first term on the right-hand-side accounts for mass transfer to/from the gas phase and the second term accounts for generation or consumption. Depending on the situation, any of the terms on the right-hand-side may be positive or negative. The mass balance considers the total inorganic carbon concentration $[C_T]$ and not just that of carbon dioxide. This is because C_T takes into account the dissolved carbon dioxide and the carbonate, CO_3^{2-}, and bicarbonate, HCO_3^-, species generated by it.

As for the liquid phase, a component mass balance can be established also for the gas; hence,

$$dF_{O_2} = -K_1 a_{1_{1O_2}}([O_2]^* - [O_2])Sdx \qquad (3)$$

$$dF_{CO_2} = -K_1 a_{1_{1CO_2}}([CO_2]^* - [CO_2])Sdx \qquad (4)$$

Here, F_{O2} and F_{CO2} are the molar flow rates of the two components in the gas phase. Note that because of the changes in molar flow rates, the volumetric flow rate of the gas phase may change along the tube. As shown later, this

change can be easily evaluated from the available equations of state for gases. This analysis assumes a constant molar flow rate for nitrogen within any section because nitrogen is neither consumed nor generated. The equilibrium concentrations of the two gases in the liquid can be calculated using Henry's law. The relevant Henry's constants for oxygen and carbon dioxide are 1.07 mol O_2 m^{-3} atm^{-1} and 38.36 mol CO_2 m^{-3} atm^{-1}, respectively, in sea water at 20°C (Doran, 1995). The vapor pressure is assumed to remain constant because of isothermal conditions. Moreover, because there are no changes in elevation within the solar receiver and frictional losses are small (smooth tube), the pressure drop along the length will be neglected and, therefore, $(P_T–P_v)$ will be considered constant.

Equations (1)–(4), which represent the model, along with the initial conditions, allow numerical integration over the loop and, hence, the determination of the CO_2 and O_2 axial profiles in the liquid phase and the molar flow rates of the two components in the gas phase. However, a relationship is needed between the total inorganic carbon concentration and the dissolved carbon dioxide in the culture. This aspect is discussed below.

Concentration of Total Inorganic Carbon in Culture

In microalgal cultures the changes in pH are due mainly to consumption of carbon dioxide; pH variations due to consumption of other nutrients and/or degradation of the excreted metabolites can be neglected. The dissolved carbon dioxide is in equilibrium with carbonate and bicarbonate species. These equilibrium are pH dependent. Loss of dissolved carbon dioxide due to uptake into algal cells is partly compensated by regeneration from carbonates and bicarbonates. Consequently, carbon dioxide uptake is accompanied by changes in pH. The relevant equilibrium and the corresponding equilibrium constants (Livansky, 1990) that need to be considered are:

$$H_2O \leftrightarrow H^+ + OH^- \qquad K_w = [OH^-] \cdot [H^+] = 10^{-14} \quad (5)$$

$$CO_2 + H_2O \leftrightarrow H_2CO_3 \leftrightarrow HCO_3^- + H^+ \qquad K_1 = [HCO_3^-] \cdot [H^+]/[CO_2] = 10^{-6.381} \quad (6)$$

$$HCO_3^- \leftrightarrow CO_3^{2-} + H^+ \qquad K_2 = [CO_3^{2-}] \cdot [H^+]/[HCO_3^-] = 10^{-10.377} \quad (7)$$

The total concentration of inorganic carbon is given by

$$[C_T] = [CO_2] + [HCO_3^-] + [CO_3^{2-}] \quad (8)$$

Combining eqs. (6)–(8), we obtain

$$d[C_T] = \left(1 + \frac{K_1}{[H^+]} + \frac{K_1K_2}{[H^+]^2}\right) d[CO_2] - [CO_2] \left(\frac{K_1}{[H^+]^2} + \frac{2K_1K_2}{[H^+]^3}\right) d[H^+] \quad (9)$$

In addition, the system must satisfy the electroneutrality constraint; thus:

$$d[H^+] + d[Cat^+] = d[OH^-] + d[HCO_3^-] + 2d[CO_3^{2-}] + d[An^-] \quad (10)$$

With this equation, assuming constant concentrations of other cations (Cat^+) and anions (An^-), and taking into account the equilibrium (5)–(7), we obtain

$$d[H^+] = \frac{\frac{K_1}{[H^+]} + 2\frac{K_1K_2}{[H^+]^2}}{1 + \frac{K_W}{[H^+]^2} + \frac{K_1[CO_2]}{[H^+]^2} + 4\frac{2K_1K_2[CO_2]}{[H^+]^3}} d[CO_2] \quad (11)$$

Equations (9) and (11) relate the three concentrations, $[H^+]$, $[C_T]$ and $[CO_2]$; knowing any one of the concentrations allows the calculation of the others.

For the riser, a piston flow pattern is also assumed, and in this case a slip velocity between the gas and the liquid phases needs to be considered. Finally, for the degasser, a stirred tank model is used and eqs. (1) to (4) are integrated for the entire degasser volume.

Predicting the Liquid Flow Rate

An important aspect of design of airlift-driven tubular photobioreactors is the ability to predict the superficial liquid velocity in the tube for various geometric and operational parameters. Liquid circulation rate controls the turbulence and shear effects in the system, determines the mixing behavior and the mass transfer capacity, and it greatly influences the axial oxygen concentration profiles in the tube. Note that eqs. (1) and (2) require knowledge of Q_L. In a design situation and in some operational situations, the liquid velocity may not be known, and a methodology is needed for its prediction from first principles. In this sense, the liquid velocity may be estimated by an extension of the well-known and widely tested model developed by Chisti (1989) for airlift devices without the solar loop.

$$U_L = \left[\frac{gh_d\varepsilon_r}{2f\frac{L_{eq}}{D}\frac{A_r}{A_d}}\right]^{0.5} \quad (12)$$

in eq. (12), f is the Fanning friction factor that can be calculated using the Blasius equation as,

$$f = 0.0791Re^{-0.25} \quad (13)$$

where Re is the Reynolds number. In the present work, the tube diameters of the riser and downcomer are equal and therefore $A_r/A_d = 1$; the equivalent length of the solar receiver loop was estimated at 118 ± 9 m, or 1.2 times the total length of the loop.

Predicting the Gas Holdup in the Reactor

As shown in eq. (12) the superficial liquid velocity is a function of gas holdup in the riser. Note that eqs. (1) and (2), and their analogous for the riser and the degasser, require knowledge of the holdup. Moreover, the gas holdup determines the mass transfer in both the airlift system and the solar receiver. Thus, to predict the gas holdup, its value in each of the reactor's zones was modeled. For the solar receiver, no slip was assumed between the liquid and the gas phases and thus, the gas holdup in the tube was calculated from the volumetric flow rates of the phases (Fig. 1) as,

$$\varepsilon_1 = \frac{Q_G}{Q_G + Q_L} \tag{14}$$

For the riser, a slip velocity exits between the gas and the liquid phases and thus, the gas holdup can be predicted by the drift flux model (Zuber and Findlay, 1965):

$$\varepsilon_r = \frac{U_{Gr}}{Co(U_{Gr} + U_{Lr}) + U_\infty} \tag{15}$$

where Co and $U\infty$ are characteristic parameters of the system. The gas holdup in the degasser is very low with respect to the riser one, and it is a function of the gas holdup in the riser,

$$\varepsilon_d = a\varepsilon_r^b \tag{16}$$

Predicting the Mass Transfer in the Reactor

The mass transfer coefficients in the system are functions of fluid dynamics in the various zones of the reactor. Because gas holdup is the principal variable that determines the mass transfer behavior of the system, the mass transfer coefficient in any zone can be predicted as a function of the gas holdup in that zone (Chisti and Moo-Young, 1987), thus,

$$K_1 a_{1_r} = a' \, \varepsilon_r^{b'} \tag{17}$$

$$K_1 a_{1_d} = a'' \, \varepsilon_d^{b''} \tag{18}$$

$$K_1 a_{11} = a''' \, \varepsilon_1^{b'''} \tag{19}$$

MATERIALS AND METHODS

The Photobioreactor

The photobioreactor, shown schematically in Figure 1, consisted of a vertical external-loop airlift pump that drove the culture fluid through the horizontal tubular solar receiver. The airlift section (riser, downcomer, and degasser) had a height of 3.5 m. The gas-injected riser and the downcomer sections (Fig. 1) were extensions of the solar receiver tube. The solar receiver was made of transparent Plexiglas tubes (0.05 m internal diameter, 0.005 m wall thickness) joined into a loop configuration by Plexiglas joints to obtain a total horizontal length of 98.8 m. The solar receiver was submerged (~ 0.05 m) in a shallow pool of water that was maintained at 21 ± 2°C by cooling (Calorex 4000 heat pump, Andrews Sykes Ltd., Malcom, Essex, England) as needed. The bottom and the inside walls of the pool were painted white to improve reflectance. The surface area of the pool was 21.4 m^2. The total culture volume in the bioreactor was 0.200 m^3.

The exhaust gas from the top of the degasser zone was analyzed for oxygen (paramagnetic analyzer) and carbon dioxide (infrared analyzer). Filter sterilized culture medium was fed in at the degasser zone. A port located on the side of the degasser section was used to continuously harvest the culture (Fig. 1). The temperature, the dissolved oxygen, and the pH measurements were made via sensors located in the degassing zone, in addition to a dissolved oxygen sensor located at the end of the external loop. The sensors were connected to a ML-4100 control unit (New Brunswick Scientific, New Brunswick, NJ) and a computer for data acquisition. Only the pH was controlled using this system; other data were monitored.

The air was supplied continuously at a flow rate of 0.0124 mol s^{-1}, whereas the CO_2 was injected under pH requirements at a flow rate of 0.0014 mol s^{-1}. The air supply point was located at the end of the loop (i.e., at the entrance of the riser), whereas CO_2 was injected, under requirement to pH control, at the entrance of the solar receiver. Both of them were continuously monitored (Fig. 1).

Microorganism and Culture Conditions

The red microalga *Porphyridium cruentum* UTEX 161 was used. The culture was operated in a continuous mode at a dilution rate of 0.050 h^{-1} applied only during 10 h in the daylight period in March 1997. During the night the dilution was stopped, and the biomass concentration declined slightly by respiration. Moreover, during the daylight period the harvest reduced the amount of biomass, hence, the biomass concentration remained almost constant throughout the day. The quasi-steady state biomass concentration attained was 3.0 $g \cdot L^{-1}$; thus, for a cumulative daily culture harvest of 100 L, the biomass productivity attained was 1.5 $g \cdot L^{-1} \cdot d^{-1}$. The pH of the culture was maintained at 7.7 by automatic injection of carbon dioxide as needed.

The culture was conducted in Hemmerick medium. The medium was fed at a constant rate during the 10-h daylight period; dilution stopped during the night. This procedure continued until biomass concentration at sunrise was the same for 4 consecutive days. All data reported were obtained after attaining the quasi-steady state. The biomass concentration was determined by dry weight. Thus, duplicate culture samples were centrifuged, washed with 0.5*M* HCl and distilled water to remove nonbiological material such as mineral salt precipitates, lyophilized for 3 d, and weighed.

The instantaneous photon-flux density of the photosynthetically active radiation (PAR) inside the thermostatic pond was measured on-line using a quantum scalar irradiance meter (LI-190 SA, Licor Instruments, Lincoln, NE,

USA) connected to the data acquisition computer. The instantaneous values were numerically integrated to obtain the daily photosynthetic photon flux density inside the pond.

The Fluid-Dynamic Parameters

The liquid velocity in the tube was measured by the tracer method. Thus, a pulse of acid/alkali was introduced at the entrance of the tubular loop and detected at the end. The liquid velocity, U_L, was calculated using the known distance L between the tracer injection and detection points (entrance and exit of the solar receiver), and the measured time interval between injection and detection. Thus,

$$U_L = \frac{L}{t_{mr}} \tag{20}$$

where the time interval t_{mr} was obtained as follows

$$t_{mr} = \frac{\int_0^\infty tCdt}{\int_0^\infty Cdt} \tag{21}$$

The gas holdup in the riser was measured by the manometric method (Chisti, 1989). Thus, two pressures taps drilled near the top and the bottom of the riser section were connected to an inverted U-tube manometer. From the known vertical distance h between the taps, and the manometer reading Δh, the holdup was calculated as follows,

$$\varepsilon_r = \frac{\Delta h}{h} \tag{22}$$

Because of the low height of the degasser, the gas holdup in this section was determined by the volume expansion method (Chisti, 1989); hence,

$$\varepsilon_d = \frac{V_d - V_d'}{V_d} \tag{23}$$

where V_d and V_d' are the volumes of the fluid in the degasser with and without aeration, respectively. Because visible gas bubbles did not recirculate, the gas holdup in the downcomer and the loop were negligible except when carbon dioxide was injected. In the latter case, the gas holdup in the loop was estimated as the ratio of the gas flow rate and the total (gas and liquid) fluid flow in the tube [eq. (14)].

Volumetric Mass Transfer Coefficients

For determining the volumetric mass transfer coefficient in the bioreactor device, the reactor was filled with seawater, and liquid circulation was initiated by supplying air in the riser as in normal culture conditions. Once a steady state had been attained, the water was air saturated and measured concentration of dissolved oxygen was constant at the entrance (i.e., in the degasser zone) and the exit of solar tube. At this point, nitrogen was injected at the inlet of the solar tube. The location of the nitrogen injection point and the flow rate of the gas were identical to those used typically with carbon dioxide during the cultures.

Because of stripping of dissolved oxygen by the nitrogen gas, the oxygen concentration at the exit of the solar tube declined continuously until a new steady state had been attained. At this condition, the amount of dissolved oxygen desorbed in the solar receiver equaled the amount of oxygen absorbed in the airlift pump (riser and degasser). An oxygen mass balance on the solar receiver could now be established as follows,

$$Q_L\,([O_2]_{in} - [O_2]_{out}) = V_1 K_1 a_{11} ([O_2{}^*] - [O_2])_{lm}\,(1 - \varepsilon_1) \tag{24}$$

In view of the plug flow regime, eq. (24) employs a logarithmic mean driving force for oxygen transfer. This is calculated as follows:

$$([O_2{}^*] - [O_2])_{lm} = \frac{([O_2{}^*]_{in} - [O_2]_{in}) - ([O_2{}^*]_{out} - [O_2]_{out})}{ln\,\dfrac{([O_2{}^*]_{in} - [O_2]_{in})}{([O_2{}^*]_{out} - [O_2]_{out})}} \tag{25}$$

The dissolved oxygen values at the inlet and the outlet of the solar tube were determined experimentally, whereas the equilibrium dissolved oxygen values were established using Henry's law. At the entrance of the solar tube (i.e., the end of the degasser), because no bubbles were present, the dissolved oxygen concentration in equilibrium with the gas phase was 0. At the exit of the solar tube, the mole fraction of oxygen in the nitrogen bubbles needed to be known to calculate $[O_2{}^*]_{out}$. The exit mole fraction of oxygen in the gas phase was calculated using

$$Q_L\,([O_2]_{in} - [O_2]_{out}) = F_{N2}\,Y_{O2,out} \tag{26}$$

where F_{N2} is the molar flow rate of the injected nitrogen and Y_{O2} is the oxygen to nitrogen molar ratio in the gas exiting from the solar receiver tube.

Similar balances could be established for the airlift pump and hence, the $K_1a_{1,\ airlift}$ in the airlift device (excluding the solar tube) could be determined. Moreover, by inserting an additional dissolved oxygen probe at the end of the riser and applying the same mass balances, the mass transfer coefficient for the riser was determined. From this value and the previously determined $K_1a_{1\ airlift}$ value the mass transfer coefficient in the degasser, $K_1a_{1\ d}$, was determined by the volumes ratio as,

$$K_1a_{1d} = \frac{K_1a_{1airlift}\,V_{airlift} - K_1a_{1r}\,V_r}{V_d} \tag{27}$$

Because for the condition studied the absorption rate was shown to be independent of the chemical reaction taking place in the liquid phase (Molina Grima et al., 1993), the $K_1a_{1\ CO2}$ could be directly related to the K_1a_1 for O_2 by a single factor (0.93) that took into account the difference in aqueous diffusivity of the two gases (Talbot et al., 1991; Molina Grima et al., 1993). Thus, using methods developed for determining O_2 absorption in gas liquid contactors it is

possible to adequately characterize CO_2 absorption for laboratory and pilot plant scale algal production systems. Moreover, as was demonstrated by earlier experiments (Contreras Gómez, 1996; Livansky and Prokes, 1973; Molina Grima et al., 1993) there exists no difference between the values of $K_l a_l$ with salt water and algae suspension in the range of concentrations used in this article. Finally, in accordance with Goldman and Dennett (1989) and Livansky (1990), the variation of the $K_l a_l$ with variation of pH along the tube was not considered because in the range of pH 6.6–8.35 they did not vary.

Photosynthesis, Oxygen Evolution, and Carbon Dioxide Consumption

The mass flow rates of ingoing air and carbon dioxide were measured by two mass flow meters (Model 824-13-0V1-PV1-V4, SIERRA Instruments Inc., Monterey, CA). A gas analyzer (Servomex Analyser Series 1400) was used to monitor the compositions of inlet and exhaust gases. The mass flow meters and the gas analyzer were connected to a data acquisition card (DaqBook/112 and DaqBoard/112, IOTECH Inc., Cleveland, OH, USA) and an IBM-compatible 486 computer for monitoring. The average rateof photosynthesis in the entire volume of the culture at any given instance was calculated using the experimentally measured gas inlet and outlet compositions and an oxygen balance. The oxygen mass balance could be written as,

$$\text{Oxygen in} + \text{Oxygen generation} = \text{Oxygen out} + \text{Oxygen accumulation} \quad (28)$$

The accumulation term could be calculated as follows:

$$\text{Oxygen accumulation} = \frac{d[O_2]}{dt} V \quad (29)$$

However, this term was lower than the difference between the oxygen inlet and exhaust (ca.. 10^{-3} mol O_2 s^{-1}) including at the first hours of light period, when the slope of dissolved oxygen is at the maximum (accumulation = $2.5 \cdot 10^{-6}$ mol O_2 s^{-1}). Thus, this term was rejected and the generation was calculated as,

$$R_{O2} = \frac{1}{V}\Delta F_{O2} = \frac{1}{V}(F_{O2\,out} - F_{O2\,in}) = \frac{F_{Air}}{V}(y_{O2\,out} - y_{O2\,in}) \quad (30)$$

In the same way, the carbon dioxide consumption was determined from the difference between the amount injected into the loop and the amount present in the exhaust gas; the accumulation term was again rejected as being negligible. Hence,

$$R_{CO2} = \frac{F_{CO2\,out} - (F_{CO2\,in} + F_{CO2\,injected})}{V} = \frac{F_{Air}(y_{CO2\,out} - y_{CO2\,in}) - F_{CO2\,injected}}{V} \quad (31)$$

Losses of Carbon Dioxide

The losses of carbon dioxide were expressed as the ratio of the net CO_2 molar flow in the exhaust gas to the molar flow injected:

$$L_{CO2} = \frac{F_{CO2\,out} - F_{CO2\,in}}{F_{CO2\,injected}} = \frac{F_{Air}(y_{CO2\,out} - y_{CO2\,in})}{F_{CO2\,injected}} \quad (32)$$

RESULTS AND DISCUSSION

Fluid-Dynamic Characterization of the System

For the fluid-dynamic characterization of the system, the variation of superficial liquid velocity, gas holdup, and mass transfer coefficients with the superficial gas velocity were studied. From the results, equations that predicted the behavior of the system were obtained and applied to simulate the scale-up characteristics. Results showed that the induced liquid circulation velocity increased with increasing aeration rate in the airlift pump. The gas holdup in the riser and degasser increased with increasing aeration rate in the riser of the airlift device. However, because of an effective gas-liquid separator, no gas bubbles were carried into the downcomer (i.e., the solar loop) under the operating conditions used (U_{gr} = 0.16 m · s^{-1}).

The gas holdup in the riser could be correlated with the superficial gas and liquid velocities in that zone using eq. (14), based on the drift flux model (Zuber and Findlay, 1965). The best- fit values of the model parameters *Co* and $U\infty$ were 0.996 and 0.651 m · s^{-1}, respectively (r^2 = 0.97). The gas holdup in the degasser was empirically correlated to the holdup in the riser,

$$\varepsilon_d = 0.24\,\varepsilon_r^{1.767} \qquad r^2 = 0.88 \quad (33)$$

The gas holdup in the solar receiver loop was negligible except when carbon dioxide was injected. For that case, the gas holdup was estimated as the ratio of the injected volumetric gas flow and the total fluid (gas + liquid) flow in the tube [eq. (14)]. Because of photosynthesis associated evolution of oxygen and absorption of carbon dioxide, the gas holdup varied slightly along the length of the solar receiver tube. This variation was taken into account by estimating the absorption/desorption from the rate of photosynthesis.

Mass Transfer

The results obtained during the determination of mass transfer coefficients in the system are displayed in Table I. The aeration rate in the riser zone influenced mainly the mass transfer in the riser and the degasser. The mass-transfer coefficient within the solar receiver tube was little affected by the aeration rate in the airlift device; instead, the rate of gas injection in the solar tube was the main factor that affected its mass-transfer coefficient. However, even for the highest gas flow rate injected (0.031 mol s^{-1}), the values of the mass transfer coefficient in the solar tube were quite low

Table I. Holdup and volumetric mass-transfer coefficients in the different zones of the bioreactor as a function of the superficial gas velocity and flow rate injected in the loop.

F_{Air}, mols^{-1}		0.0186			0.0248			0.0310	
F_{N2}, mols^{-1}	0.0006	0.0012	0.0019	0.0006	0.0012	0.0019	0.0006	0.0012	0.0019
U_{gr}, ms^{-1}	0.2193	0.2264	0.2341	0.2900	0.2971	0.3049	0.3608	0.3678	0.3756
U_{lr}, ms^{-1}	0.4246	0.4301	0.4359	0.4750	0.4796	0.4846	0.5184	0.5225	0.5269
$[O_2]_l$[a]	0.8401	0.7072	0.6345	0.8530	0.7453	0.6769	0.8703	0.7693	0.7020
$[O_2]_r$[a]	0.8883	0.7993	0.7474	0.8974	0.8262	0.7794	0.9093	0.8480	0.8059
$[O_2]_d$[a]	0.9055	0.8295	0.7830	0.9144	0.8530	0.8114	0.9251	0.8736	0.8365
ε_l	0.0164	0.0318	0.0479	0.0147	0.0287	0.0433	0.0135	0.0264	0.0400
ε_r	0.1695	0.1734	0.1776	0.2061	0.2095	0.2132	0.2383	0.2413	0.2446
ε^d	0.0104	0.0108	0.0113	0.0147	0.0151	0.0156	0.0190	0.0194	0.0199
K_la_{11}, s^{-1}	0.0003	0.0008	0.0010	0.0004	0.0007	0.0010	0.0003	0.0007	0.0010
K_1a_{1r}, s^{-1}	0.0770	0.0840	0.0898	0.0859	0.0957	0.1026	0.0954	0.1156	0.1262
$K_1a_{1\ airlift}$, s^{-1}	0.0193	0.0207	0.0219	0.0217	0.0233	0.0247	0.0243	0.0279	0.0298
$K_1a_{1\ d}$, s^{-1}	0.0070	0.0071	0.0074	0.0079	0.0078	0.0080	0.0090	0.0092	0.0092

[a]With regard to saturation with air.

(e.g., $K_la_{l\ l} = 0.0010$ s^{-1}), suggesting that this variable possibly limited the mass-transfer capability of the system in the solar receiver.

The K_la_l values in the airlift device, $K_la_{l\ airlift}$, were much greater than in the solar loop. This good mass-transfer capability of the airlift zone contributed to effective removal of oxygen from the culture. Thus, whereas the culture returning from the solar loop contained about 300% oversaturation with air (0.67 mol m^{-3} of dissolved oxygen), the oxygen content of the returning fluid was reduced to 130% (0.3 mol m^{-3}). This oxygen removal is similar to that achieved by Richmond et al. (1993) in cultures of the cyanobacteria *Spirullina platensis* and *Anabaena siamensis* in a parallel flow tubular reactor. Typically, the O_2 concentration measured at the inlet of the airlift system was found to reach 0.52 mol m^{-3}, whereas at the outlet the concentration was 0.32 mol m^{-3} (Richmond et al., 1993). Note that the K_la_l values in the airlift zone are relatively low in comparison with published data (Chisti, 1989) for airlift bioreactors; therefore, the scope for improvement is substantial. For example, for a superficial air velocity of 0.16 m s^{-1} Contreras Gómez (1996) reported a K_la_l value in salt water (0.028 s^{-1}) that was about 51% greater than the value seen in our case. This low value of K_la_l is due to slug flow in the riser and hence, a relatively low interfacial area. Also, the K_la_l in external-loop reactors is generally lower than in bubble column or internal-loops because the downcomer or external loop is virtually gas free.

The measured gas-liquid volumetric mass transfer coefficients in the riser, degasser, and the solar loop could be correlated with the gas holdup in those zones as follows,

$$K_1a_{11} = 0.0213\ \varepsilon_1^{0.9694} \qquad r^2 = 0.9653 \qquad (34)$$

$$K_1a_{1_r} = 0.4098\ \varepsilon_r^{0.9204} \qquad r^2 = 0.8173 \qquad (35)$$

$$K_1a_{1_d} = 0.04519\ \varepsilon_d^{0.41} \qquad r^2 = 0.9542 \qquad (36)$$

Similar relationships between K_la_l and gas holdup have been published before (Chisti, 1989), and they suggest that the gas-liquid interfacial area is the principal factor influencing the overall mass transfer coefficient. Indeed, the exponents on the gas holdup terms in eqs. (34)–(36) are consistent with the values noted by (Chisti et al., 1987).

Mixing

In a photobioreactor that was geometrically similar to the one used here, the measured Peclet numbers, $D_{xi}/(U_iL)$, for the horizontal tube and the airlift zone (riser and degasser) were 2500, 4.2, respectively, for operating conditions similar to the ones employed in this work. Because the defining criteria for plug flow requires that Peclet number exceed 20 (Pavlica and Olson, 1970), the flow the in solar receiver was clearly a well-developed plug flow. The airlift section was more axially mixed, but even this zone could not be considered fully backmixed because the Pe was far greater than 0.1, which is when a fully backmixed state can be assumed (Pavlica and Olson, 1970).

Application of the Model for Prediction of Culture Behavior

The oxygen-generation rate in the bioreactor was determined in continuous culture at steady state. In the proposed mathematical model the time variation of the photosynthesis rate is not considered. However, the model allows simulating the behavior of the system along the day because the time variation of the photosynthesis rate is slow, and for short-time intervals an average value could be assumed. Moreover, if the time variation of the photosynthesis rate is known, the model predicts the culture variables as dissolved oxygen, carbon content within the culture, composition of the gas outlet, carbon dioxide losses and requirements, and pH of the culture. The proposed model does not consider the position dependence of the rate of photosynthesis in the solar tube: Photosynthesis is assumed to occur at a fixed average rate everywhere in the tube, but that average rate varies with time during the day. This simplification is jus-

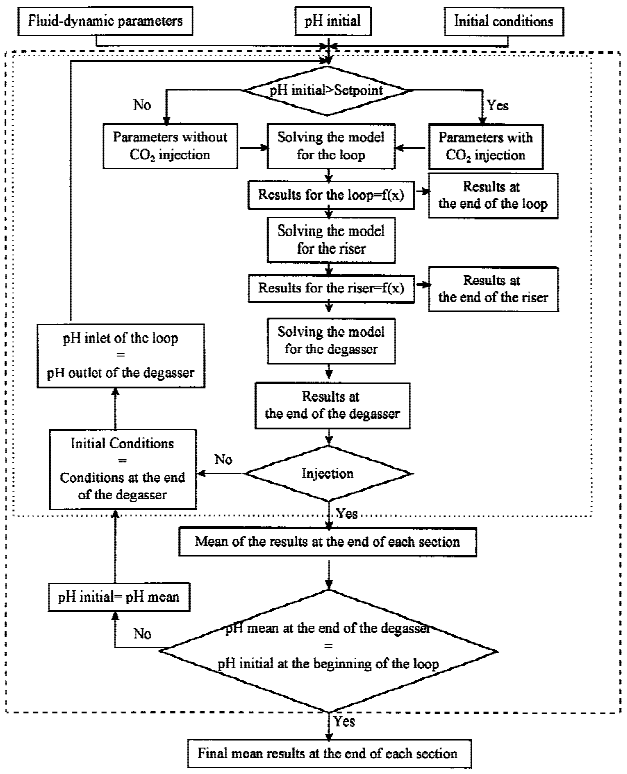

Figure 2. Computational flowchart used for the simulations.

tified because: (1) the microalgae grow slowly and cell concentration changes little during the residence time in a 100-m tube as in this work; (2) a 100-m continuous tube run is about the maximum that can sensibly be used in tubular photobioreactor because of oxygen build-up; and (3) the change in incidence photon-flux density at the surface of the solar receiver is quite small over the period of one residence time (~ 4 min) in the tube. Although a 100-m tube was used in this work, the achieved length will depend also on the specific tube diameter. Despite the simplifying assumption, the model satisfactorily simulates the behavior of the system as demonstrated later in this section.

Figure 2 shows the computational flowchart utilized. From experimental values of fluid-dynamic parameters and the photosynthesis rate, and any estimated initial conditions of the culture (pH, dissolved oxygen, dissolved total inorganic carbon) the computational program compares if the pH is higher than setpoint or not. If not, the calculations are done without considering CO_2 injection. If injection is indicated, the same equations are solved but the parameters that take into account the CO_2 injection are utilized. An iterative calculation procedure is followed until the solution converges to a constant pH.

Regarding the supply of carbon dioxide, two situations need to be examined. In the first case, the pH increases to above the setpoint because of consumption of carbon dioxide by the cells, and, in response, carbon dioxide is injected into the solar loop. The second situation occurs when the pH declines to below the setpoint and carbon dioxide injection ceases. The proposed model simulates the behavior of the system in both those situations as shown in Figures 3 and 4. When the pH is higher than the setpoint and CO_2 is being injected (Fig. 3), the model predicts an increase in dissolved oxygen to 0.67 mol m^{-3} (ca.. 300% over saturation with respect to air) at the end of the loop. As the fluid enters the riser, the oxygen concentration declines rapidly because oxygen is stripped by the injected air. The same effect continues in the degasser zone. Consequently, the dissolved oxygen concentration in the fluid returning to the solar loop drops to 0.3 mol $O_2 \cdot m^{-3}$, which is the same as at the beginning of the solar loop cycle.

The concentration of carbon dioxide in the culture increases initially because of absorption from the injected bubbles; however, the increase does not persist for long because some of the oxygen from the supersaturated liquid transfer to the carbon dioxide gas phase which is diluted sufficiently so that there is no build-up in the liquid. Thus, halfway down the solar loop, the rate of absorption of CO_2 becomes lower than consumption by photosynthesis; hence, the dissolved CO_2 level actually drops a little. In the riser and the degasser, the carbon dioxide level drops faster because it is rapidly stripped by air where the carbon dioxide partial pressure is only 0.03% compared to 2.61% in the returning culture. Concentration of CO_2 at aprroximately

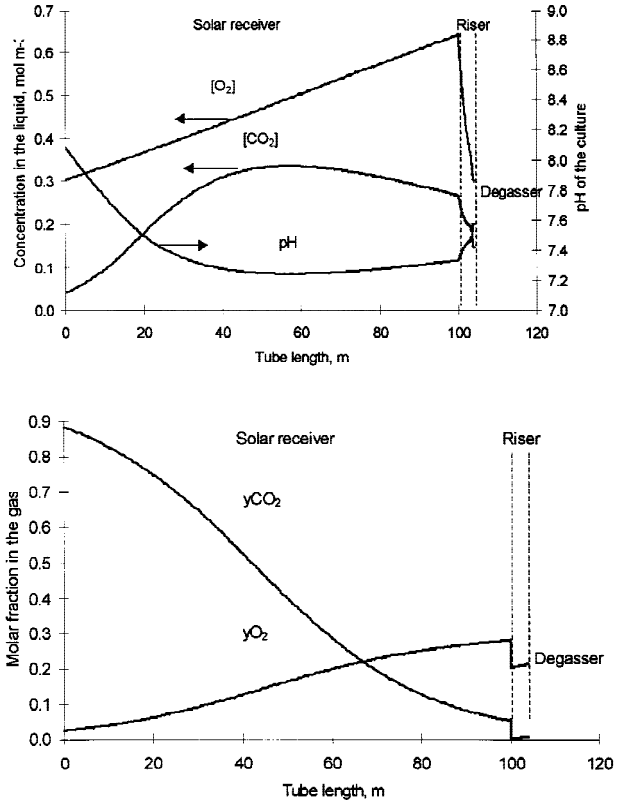

Figure 3. Variation of oxygen and carbon dioxide concentrations in liquid and gas phases, and the culture pH when pure carbon dioxide is injected in the loop, at 12:00 solar hour. Length of solar receiver = 98.8 m; culture circulation rate = $9.7 \cdot 10^{-4}$ m^3 s^{-1}; gas injection rate in the solar receiver = $2.5 \cdot 10^{-5}$ m^3 s^{-1}; biomass concentration = 3.0 g L^{-1}.

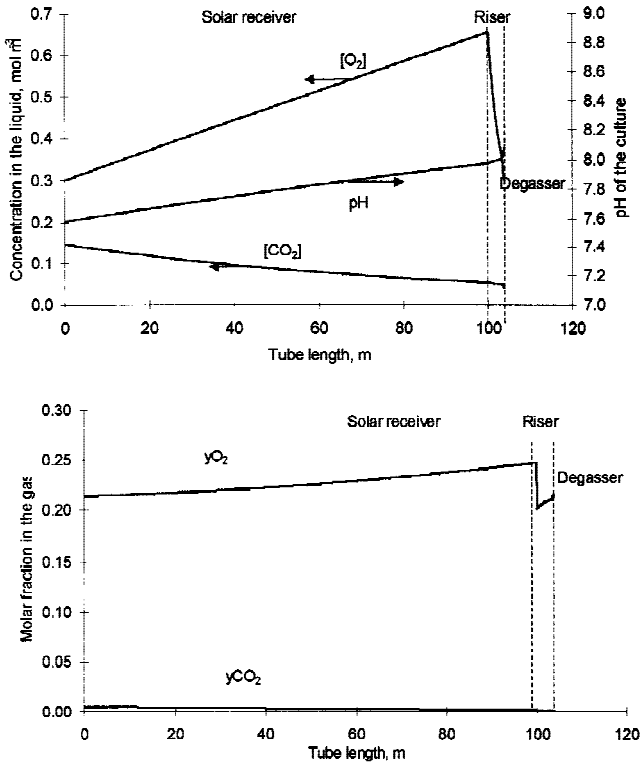

Figure 4. Variation of oxygen and carbon dioxide concentrations in liquid and gas phases, and culture pH when pure carbon dioxide is not injected in the loop, at 12:00 solar hour. Length of solar receiver = 98.8 m; culture circulation rate = $9.7 \cdot 10^{-4}$ m^3 s^{-1}; gas injection rate in the solar receiver = $2.5 \cdot 10^{-5}$ m^3 s^{-1}; biomass concentration = 3.0 g L^{-1}.

1.5 mol m^{-3} has been suggested to inhibit certain cultures of microalgae (Lee and Hing, 1989). In our case, even when pure CO_2 was injected the CO_2 concentration never exceeded those values, thus inhibition by this nutrient could be neglected.

The culture pH profile simply complements that of carbon dioxide: pH declines with absorption of carbon dioxide and rises when carbon dioxide is stripped. The gas-phase concentration profiles too, simply complement those discussed above for the culture fluid.

In the situation when carbon dioxide is not injected (Fig. 4), the concentration profiles are different. Because of photosynthetic generation, the oxygen concentration rises steadily, whereas the dissolved carbon dioxide level drops steadily as the gas is consumed. Again, the pH profile simply compliments that of the dissolved carbon dioxide. The pH rises and, to maintain its value at the desired setpoint, some carbon dioxide needs to be injected on alternate cycles. The higher the rate of photosynthesis, the more frequent are the carbon dioxide injections.

The culture was conducted with pH control that relied on injecting carbon dioxide as short bursts under requirements at a flow rate of 0.0012 mol s^{-1}. The model was applied repeatedly throughout the day following the flowchart depicted in Figure 2 and considering the actual photosynthesis rate at each period of time. This method allowed determination of the injection/no injection time ratio and the total carbon injected.

The simulated results were compared to the experimental

Table II. Hourly mean values of culture variables for the steady state reached at 0.05 h^{-1} in March 1997.

Hour	y_{O2}, gas	y_{CO2}, gas	Q_{CO2}, g min^{-1}	I, $\mu Em^{-2}s^{-1}$	G, Wm^{-2}	R_{O2}, mol $m^{-3}s^{-1}$	R_{CO2}, mol $m^{-3}s^{-1}$	CO_2 loss, %	$[O_2]_d$ % Sat.	$[O_2]_l$ % Sat.	pH
0	0.199	0.005	0.253	7	4	−0.0002	0.0003	132.0	77.0	74.0	7.54
1	0.199	0.005	0.255	7	5	−0.0002	0.0001	124.0	80.7	73.0	7.50
2	0.199	0.005	0.257	8	6	−0.0002	0.0000	127.3	81.6	74.0	7.55
3	0.199	0.005	0.259	8	5	−0.0002	0.0003	124.0	84.4	74.0	7.55
4	0.199	0.005	0.246	8	6	−0.0002	0.0001	124.5	84.8	75.0	7.49
5	0.199	0.005	0.265	10	6	−0.0002	0.0000	129.9	84.8	75.0	7.52
6	0.199	0.005	0.263	75	22	−0.0002	0.0001	122.0	90.7	80.0	7.53
7	0.202	0.005	0.493	561	147	0.0002	−0.0003	66.2	98.5	125.0	7.61
8	0.205	0.004	0.733	1277	298	0.0006	−0.0008	37.7	104.9	175.0	7.66
9	0.211	0.004	0.906	3235	715	0.0014	−0.0013	26.4	124.9	282.0	7.66
10	0.212	0.004	1.010	3842	874	0.0016	−0.0015	21.9	129.9	290.0	7.54
11	0.213	0.004	1.055	3724	966	0.0017	−0.0016	19.1	135.5	300.0	7.55
12	0.213	0.003	1.133	3954	980	0.0018	−0.0018	16.4	137.9	312.0	7.85
13	0.213	0.003	1.080	3662	913	0.0017	−0.0017	16.9	132.0	300.0	7.64
14	0.212	0.003	1.088	3059	772	0.0016	−0.0017	19.2	127.0	290.0	7.72
15	0.210	0.004	1.012	1925	580	0.0013	−0.0015	25.0	122.0	278.8	7.66
16	0.206	0.004	0.739	831	354	0.0008	−0.0010	35.8	105.5	190.0	7.64
17	0.202	0.005	0.414	232	128	0.0002	−0.0002	68.3	92.5	120.5	7.59
18	0.199	0.005	0.250	25	9	−0.0002	0.0001	126.9	80.5	80.0	7.50
19	0.199	0.005	0.253	6	4	−0.0002	0.0000	125.5	82.2	73.2	7.56
20	0.199	0.005	0.253	6	4	−0.0002	0.0002	125.0	83.5	73.0	7.51
21	0.199	0.005	0.257	6	4	−0.0002	0.0001	121.0	85.0	73.0	7.53
22	0.199	0.005	0.255	7	4	−0.0002	0.0003	128.0	86.5	73.0	7.56
23	0.199	0.005	0.250	7	4	−0.0002	0.0001	122.4	77.5	73.0	7.54

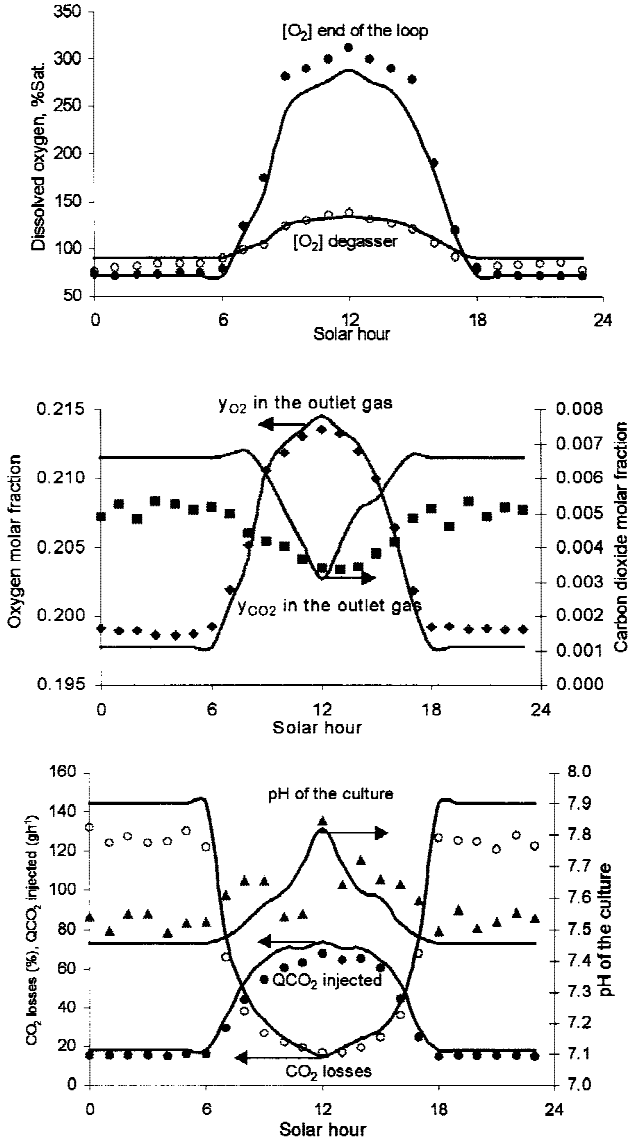

Figure 5. Comparison between experimental (points) and simulated (lines) data. Length of solar receiver = 98.8 m; culture circulation rate = $9.7 \cdot 10^{-4}$ m^3 s^{-1}; gas injection rate in the solar receiver = $2.5 \cdot 10^{-5}$ m^3 s^{-1}; biomass concentration = 3.0 g L^{-1}.

data (Table II) to verify the predictive capabilities of the model. As shown in Figure 5, throughout any 24-h period, the simulated data—pH, carbon dioxide losses, and the amount of carbon dioxide injected—closely agreed with the measurements. Although the simulations reproduced the measurements, the closeness of fit depended on the variable being predicted. Significantly, in all cases the predicted and observed qualitative behaviors were quite consistent.

Ideally, the correlation between simulated and experimental data should be linear: A parity plot should have a unit slope and zero intercept. As shown in Figure 6, the normalized (value/maximum of values) experimental observations and the simulations generally correlate well. Although, the degree of correlation differs for different variables, the mean of the errors for the entire set of variables is lower than 15% (mean standard deviation lower than 8%). Clearly, the model is sufficiently reliable for predicting behavior of a range of parameters all through the culture period.

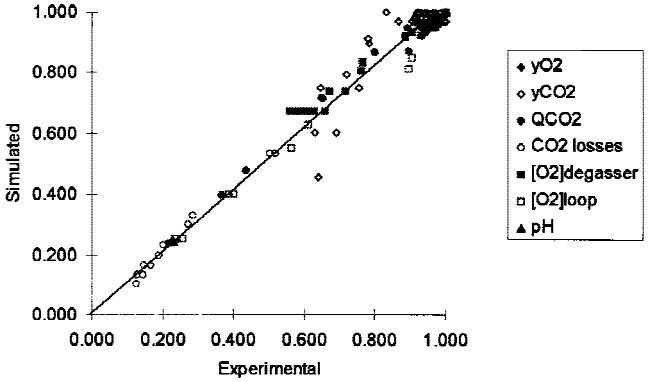

Figure 6. Parity plot of simulated vs. normalized experimental data. Length of solar receiver = 98.8 m; culture circulation rate = $9.7 \cdot 10^{-4}$ m^3 s^{-1}; gas injection rate in the solar receiver = $2.5 \cdot 10^{-5}$ m^3 s^{-1}; biomass concentration = 3.0 g L^{-1}.

As shown in Figures 5 and 7, during the daylight period

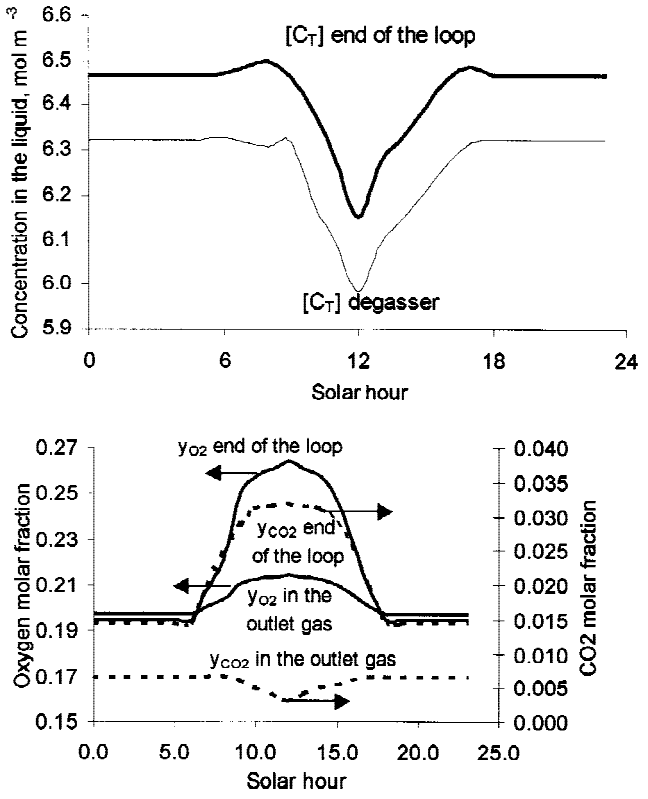

Figure 7. Variation of total inorganic carbon in the liquid, and oxygen and carbon dioxide molar fraction in the gas at the end of the loop and in the degasser with the solar hour. Length of solar receiver = 98.8 m; culture circulation rate = $9.7 \cdot 10^{-4}$ m^3 s^{-1}; gas injection rate in the solar receiver = $2.5 \cdot 10^{-5}$ m^3 s^{-1}; biomass concentration = 3.0 g L^{-1}.

the dissolved oxygen builds up to very high levels: 0.674 mol $O_2 \cdot m^{-3}$, or ca. 300% oversaturation at the end of the solar loop; and 0.281 mol $O_2 \cdot m^{-3}$, or ca. 125% oversaturation in the degasser. This suggests that a strategy for dissolved oxygen control should be based on measurements at the end of the solar loop where concentration is highest; dissolved oxygen measurements in the degasser zone, a frequent practice used also in this work, are less satisfactory as they do not reflect the dangerously high levels that occur in the system.

Further evident from Figure 5 is the model's capacity to predict the amount of carbon dioxide injected to control pH, the average pH of the culture, and the amount of carbon dioxide lost. The results show (Fig. 5) that the pH varied during the course of culture from 7.46 during the night to 7.82 at mid-day. The rise was due to increased carbon dioxide consumption during the day. Although the pH-control system attempted to reduce the pH by more frequently injecting the gas, the maximum injection rate was deliberately set low to prevent too much loss of carbon dioxide. Of course, a suitable control system would have automatically adjusted the length of the injection burst, but the control strategy relied on a basic on–off approach that modified only the frequency of burst, but not the rate of gas flow.

Once the predictive ability of the model had been exhaustively demonstrated for a variety of parameters, it was used to simulate the behavior of other parameters that were not directly measured. The aim was to gain further insight into the culture behavior. Thus, as shown by simulations in Figure 7, total concentration of inorganic carbon in the cell-free culture coming out of the solar receiver tube declined during the daylight hours because of consumption by photosynthesis. The concentrations were higher during the night because of respirative release of carbon dioxide (Fig. 7). Simulated behavior in degasser was similar to that in the solar receiver.

Similarly, the deduced composition of the gas phase in various zones of the reactors is shown in Figure 7 as a function of time. During the light period, the oxygen mole fraction in the gas phase exiting the solar loop is higher than in exhaust gas from the reactor. This is because the gas from the solar tube is diluted by the air injected in the riser before being exhausted. For carbon dioxide (Fig. 7), during daylight, the mole fraction in the gas phase is high at the end of the solar loop (10 times higher than the mole fraction in the atmosphere), because more gas is injected to control the pH. However, in the exhaust gas the carbon dioxide concentration is almost the same as in the normal atmosphere. This is the result of dilution by the air in the riser, and the fact that the gas-phase volume flow leaving the solar loop is negligibly small compared to the air injected into the riser. Because the gas-phase concentration of carbon dioxide is quite low in the airlift pump, the liquid returning to the solar loop is also proportionately low in dissolved carbon dioxide. Note, however, that the carbon dioxide concentration in the exhaust gas is slightly lower during daylight period than during the night hours. This is because of respiratory generation of carbon dioxide throughout the culture during the night.

Application of the Model for Scale-Up and Optimization

In view of its predictive capability, the model may be used as a scale-up and optimization tool to evaluate the influence of various design variables on expected performance. For example, increasing the length of the continuous-run solar receiver tube or the flow rate through the tube (i.e., increasing the superficial gas velocity in the riser of the airlift pump) will influence the dissolved oxygen and carbon dioxide concentration profiles through the solar tube. The proposed model can quantitatively predict the specific profile changes, the induced liquid velocity in the solar tube for any specified aeration rate in the riser, the consequent changes in gas holdup and the gas-liquid mass transfer characteristics of the various zones (Fig. 8). The effects of varying the carbon dioxide concentration in the gas injected into the solar loop can be simulated and the losses of carbon dioxide in the exhaust gas can be predicted.

The simulations spanned the following ranges: 50–150 m variation in length of continuous-run solar tube; 25–45 $L \cdot min^{-1}$ change in air-flow rate in the riser; 70–110 $L \cdot h^{-1}$ variation in the pH-control gas injection rate in the solar loop; and 0.4–1.0 change in the carbon dioxide mole fraction in the pH control gas. Various combinations of those ranges resulted in a total of 875 simulations. For each case, the following parameters were computed: the mean value of carbon dioxide loss, the culture pH, the carbon dioxide supplied, the dissolved oxygen and carbon dioxide concentra-

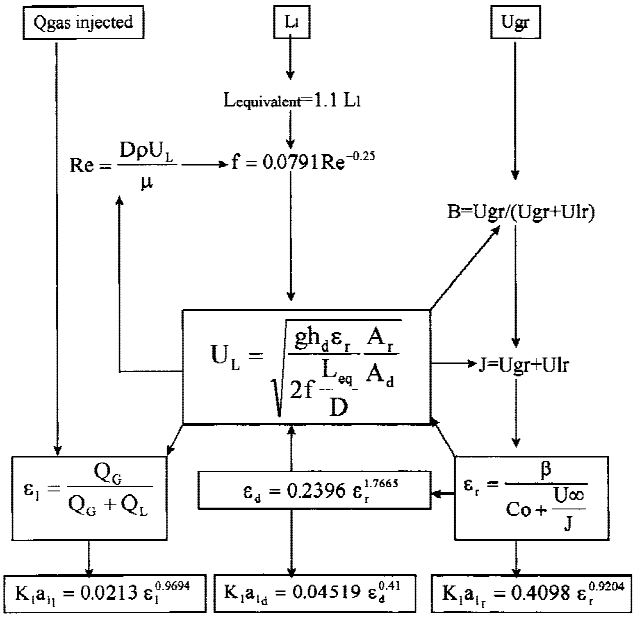

Figure 8. Equations used to simulate the variation of fluid-dynamic parameters when loop length, superficial gas velocity, or gas flow injected modifies.

tions at the end of the solar loop and in the degasser, and the total inorganic carbon concentration.

To characterize the influence of the earlier specified variables, the entire simulated data was subjected to analysis-of-variance (ANOVA). Values of the *F*-ratio and significance levels were obtained (Table III) as well as the mean values and standard deviations due to variation of the other simulated parameters. As shown in Table III, the length of the solar loop is the principal variable that influences the systems behavior: The *F*-ratio values and significance levels are generally highest with regard to the impact of loop length on carbon losses, pH, the amount of carbon dioxide supplied, the oxygen concentration at the end of the loop, and the total inorganic carbon in the cell-free culture. As seen in Figure 9, the higher the loop length the lower the carbon losses in the system and the higher the dissolved oxygen at the end of the loop. The increase in dissolved oxygen is due to increased residence time in the tube. At the end of a 150 m tube, the oxygen builds up to more than 300% oversaturation (0.76 mol $O_2 \cdot m^{-3}$) (Fig. 9). In practice, of course, the rate of increase along the tube would depend on the specific microalgae. Also, at such high concentrations, the predicted linear increase in dissolved oxygen may not occur, because the assumption of constant rate of photosynthesis will breakdown. For long tubes, the oxygen may build-up to inhibitory levels and the rate of photosynthesis will decline. Moreover, for a long tube the culture will require higher airlift devices and therefore, higher air pressure. Besides, the culture density along the tube will vary significantly and, again, the self-shading effect that is not considered here will reduce the rate of photosynthesis. This constraint may be reduced in parallel-flow tubular reactors that use manifolds to connect several tubes in parallel (Richmond et al., 1993). The simulations presented here provide a useful starting point for bioreactor design.

Based on the simulations (Fig. 9), the carbon loss declines with increasing length of the solar tube. Whereas up to 30% of the injected carbon dioxide would be lost in a system with a 50-m long solar receiver, the losses could be reduced to about 5% if the length were increased to 150 m.

Table III. F-ratio and statistical significance of both design (length of the solar receiver) and operation variables (air flow in the riser, gas flow injected in the solar receiver, and composition) obtained from statistical variance analysis of simulated data.

	Loop length	Air flow	Gas flow injected	CO_2 molar fraction
Carbon losses	325.4[b]	7.712[b]	4.092[a]	27.270[b]
pH	49.876[b]	0.166	15.870[b]	53.820[b]
CO_2 supply	84.035[b]	0.968	8.570[b]	117.462[b]
$[O_2]_{in}$	38.126[b]	926.03[b]	0.018	1.180
$[O_2]_{out}$	3627.2[b]	9.941[b]	0.066	5.651[b]
$[C_T]_{in}$	108.997[b]	0.061	0.387	60.815[b]
$[C_T]_{out}$	104.400[b]	0.067	0.413	63.186[b]

[a]Significance higher than 95.0%.

[b]Significance higher than 99.9% in, entrance of the solar receiver out, exit of the solar receiver.

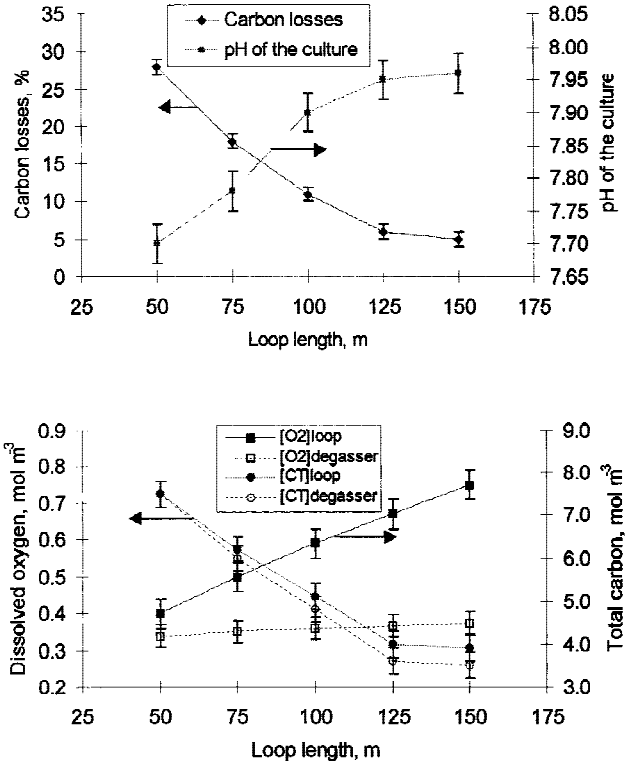

Figure 9. Influence of loop length on the behavior of the system. The error bars represent the standard deviation of the simulated data by the modification of the other variables studied.

This is simply because a longer tube allows more gas-liquid contact time for mass transfer. These lower carbon losses imply that the culture would be approaching carbon limitation and the pH at the end of the loop would rise to 8.0 from the setpoint value of 7.7.

Furthermore, the composition of injected gas also greatly affects the carbon losses, the pH of the culture, and the total inorganic carbon in the system (Table III). The lower the carbon dioxide mole fraction in the gas injected for pH control, the lower are the carbon losses, but the pH of the culture is higher (Fig. 10). Significantly, decreasing the carbon dioxide mole fraction in the injected gas from 1.0 (pure carbon dioxide) to 0.4, reduces carbon loss from 20% to only 7% of the injected gas (Fig. 10).

CONCLUSIONS

Tubular photobioreactors are a promising design for highly controlled, large-scale culture of microalgae. Suitably designed tubular solar receivers effectively harvest much of the sunlight impinging on the reactor surface; they allow enhanced yield and monoalgal cultivation. Unlike the widely used open-culture systems (Livansky and Bartos, 1986; Livansky, 1982, 1990; Märkl and Mather, 1987; Weissman et al., 1988), the design of closed tubular photobioreactors is more complex, and the basic knowledge required for predictable performance is only now beginning to

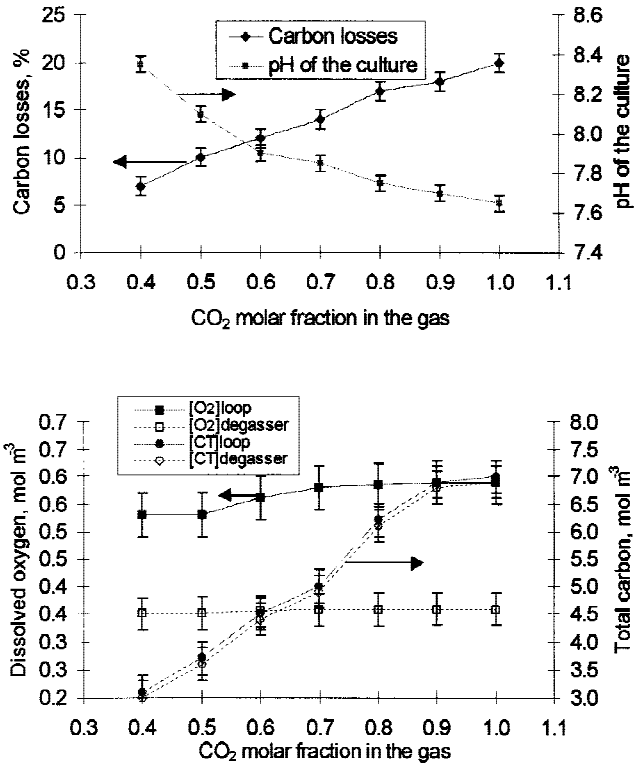

Figure 10. Influence of CO_2 composition of injected gas on the behavior of the system. The error bars represent the standard deviation of the simulated data by the modification of the others studied variables.

emerge. This work addresses the principal aspects of tubular photobioreactor design, including build-up and removal of photosynthetically generated oxygen, the efficient utilization of the expensive carbon dioxide, and the effects of liquid velocity on concentration profiles of those gases in the solar tube. A model is developed for predicting the oxygen and carbon dioxide profiles in liquid and gas phases. The model is shown to apply during continuous-outdoor culture of *Porphyridium cruentum* in a 200-L photobioreactor with a 100-m solar receiver tube. The predictive capabilities of the developed model suggest its potential as a scale-up tool. The model presented is simple and can be adapted to other types of tubular photobioreactors and photoautotrophic strains.

Loss of the expensive carbon dioxide can be reduced simply by switching off the CO_2-based pH control loop during the dark hours when photosynthesis ceases. During the night, cells of microalgae actually produce carbon dioxide. During daytime, reducing carbon dioxide loss requires improvement of the gas-liquid volumetric mass-transfer coefficient inside the solar loop. Furthermore, to aid stripping of accumulated inhibitory oxygen, high $k_l a_l$ values are necessary in the airlift device where the residence time must be low, because the photosynthetic productivity of the airlift zone per se is relatively minor. In a continuous-run solar tube, oxygen accumulation to inhibitory levels is clearly the major problem. Irrespective of the fluid dynamics, the dissolved carbon dioxide levels can be easily maintained between 1 and $6 \cdot 10^{-3} M$, or 1000-fold greater than the critical concentration reported by Märkl and Mather (1985) and Weissman et al. (1988) for optimal productivity of *Chlorella vulgaris* and saline diatoms, respectively. Similarly, the minimum requirements of $2.4 \cdot 10^{-3} M$ carbon dioxide for maximum growth rate of 0.041 h^{-1} in cultures of *Tetraselmis* can be easily maintained (Olaizola et al., 1991).

The authors thank Dr. Livansky for his comments on the draft of the manuscript. Thanks are also due to Professor Y. Chisti for helpful discussions during the manuscript's final draft.

NOMENCLATURE

$[CO_2]$	dissolved carbon dioxide concentration in the liquid, mol m^{-3}
$[C_T]$	dissolved total inorganic carbon concentration in the liquid, mol m^{-3}
$[H^+]$	proton concentration in the liquid, mol m^{-3}
$[O_2]$	dissolved oxygen concentration in the liquid, mol m^{-3}
$[O_2]_{in}$	dissolved oxygen concentration at the beginning of the loop, mol m^{-3}
$[O_2]_{out}$	dissolved oxygen concentration at the end of the loop, mol m^{-3}
$[OH^-]$	hydroxyl concentration in the liquid, mol m^{-3}
A_d	cross-section of the downcomer, m^2
A_r	cross-section of the riser, m^2
Cb	biomass concentration, g L^{-1}
Co	drift flux model parameter [eq. (15)]
D	tube diameter, m
f	Fanning friction factor
F_{Air}	air molar flow rate supplied to the riser, mol s^{-1}
F_{CO2}	carbon dioxide molar flow rate in the gas phase, mol s^{-1}
F_{O2}	oxygen molar flow rate in the gas phase, mol s^{-1}
G	daily averaged global irradiance on the pond surface, W m^{-2}
h	vertical distance between the manometer taps in the riser, m
H_{CO2}	carbon dioxide Henry's law constant, mol m^{-3} atm^{-1}
h_D	height at which the degasser is situated, m
H_{O2}	oxygen Henry's law constant, mol $m^{-3}atm^{-1}$
I	photon-flux density photosynthetically active radiation inside the pond, μEm^{-2} s^{-1}
K_1	first equilibrium constant for bicarbonates buffer, mol m^{-3}
K_2	second equilibrium constant for bicarbonates buffer, mol m^{-3}
$K_l a_{l,l}$	mass transfer coefficient for the liquid phase in the solar receiver, s^{-1}
$K_l a_{ld}$	mass transfer coefficient for the liquid phase in the degasser, s^{-1}
$K_l a_{lr}$	mass transfer coefficient for the liquid phase in the riser, s^{-1}
K_W	hydrolysis constant of the water
L	distance between the tracer injection and detection points
L_{CO2}	carbon losses in the system, %
P_T	total pressure in the system, atm
P_v	water partial pressure in the gas phase, atm
Q_G	volumetric gas flow rate, m^3 s^{-1}
Q_L	volumetric liquid flow rate, m^3 s^{-1}
R_{CO2}	carbon dioxide generation rate of the culture, mol O_2 m^{-3} s^{-1}
R_{O2}	oxygen generation rate of the culture, mol O_2 m^{-3} s^{-1}
S	cross-section of the tube, m^2
t_{mr}	time interval between tracer injection and detection, s
$U\infty$	drift flux model parameter, m s^{-1} [eq.(27)]
U_L	superficial liquid velocity in the tube, m s^{-1}
U_{Gr}	superficial gas velocity, m s^{-1}
V_d	volume of gas-liquid dispersion in the degasser, m^3
V_d'	unaerated liquid volume in the degasser, m^3
V_L	volume of gas-liquid dispersion in the solar receiver, m^3

y_O oxygen molar fraction in the gas phase
Y_O oxygen to nitrogen molar ration in the gas phase, mol O_2 mol N_2^{-1}
μ viscosity of liquid, kg m^{-1} s^{-1}
ϵ_d gas holdup in the degasser
Δh manometer reading, m
ρ_L density of liquid, kg m^{-3}
ϵ_i gas holdup in the solar receiver
ϵ_r gas holdup in the riser

References

Acién Fernández FG, García Camacho F, Sánchez Pérez JA, Fernández Sevilla JM, Molina Grima E. 1997. A model for light distribution and average solar irradiance inside outdoor tubular photobioreactors for the microalgal mass culture. Biotech Bioeng 55:701–712.

Acién Fernández FG, García Camacho F, Sánchez Pérez JA, Fernández Sevilla JM, Molina Grima E. 1998. Modeling of biomass productivity in tubular photobioreactors for microalgal cultures. Effects of dilution rate, tube diameter and solar irradiance. Biotechnol Bioeng, in press.

Aiba S. 1982. Growth kinetics of photosynthetic microorganisms. Adv Biochem Eng 23:85–156.

Borowitzka MA. 1996. Closed algal photobioreactors: Design considerations for large-scale systems. J Mar Biotechnol 4:185–191.

Colman B, Rotatore C. 1995. Photosynthetic inorganic carbon uptake and accumulation in two marine diatoms. Plant Cell and Environment 18: 919–924.

Contreras Gómez A. 1996. Caracterización de una columna de burbujeo con recirculación interna. Aplicación al cultivo de Phaeodactylum tricornutum. Ph.D. Thesis, Universidad de Almería, Spain.

Coulson JM, Richardson JF. 1990. Chemical engineering, Vol. 1., 4th edition. Oxford: Pergamon Press. pp 45–110.

Chisti MY. 1989. Airlift bioreactors. Elsevier Science Publishers, London.

Chisti MY, Moo-Young M. 1987. Airlift reactors: Characteristics, applications and design considerations. Chem Eng Commun 60:195–242.

Chisti MY, Halard B, Moo-Young M. 1988. Liquid circulation in airlift reactors. Chem Eng Sci 43:451–457.

Doran PM 1995. Bioprocess engineering principles. San Diego: Academic Press. p 208–209.

Fraser RD, Ritchie BJ, Hill GA. 1994. Dynamic mixing and oxygen transfer in small, airlift loop bioreactors: Model and experimental verification. Biotechnol Prog 10:543–547.

Goldman JC, Dennett MR. 1983. Carbon dioxide exchange between air and sea water: No evidence for rate catalysis. Science 220:199–201.

Gudin C, Therpenier C. 1986. Bioconversion of solar energy into organic chemicals by microalgae. In: Mizrahi A, editor. Advances in biotechnological processes. New York: Alan Liss. Vol. 6. p 73–110.

Gudin C, Chaumont D. 1983. Solar biotechnology study and development of tubular solar receptors for controlled production of photosynthetic cellular biomass. In: W. Palz and D. Pirrwitz, editor. Proceedings of the workshop and EC contractors' meeting in Capri. The Netherlands: Reidel Publ. Co., Dordrecht, pp 184–193.

Ho CS, Erickson LE, Fan LT. 1977. Modeling and simulation of oxygen transfer in airlift fermentors. Biotechnol Bioeng 19:1503–1522.

Lee YK. 1986. Enclosed bioreactor for the mass cultivation of photosynthetic microorganisms: The future trend. TIBTECH 4:186–189.

Lee YK, Hing HK. 1989. Supplying CO_2 to photosynthetic algal cultures by diffusion through gas-permeable membranes. Appl Microbiol Biotechnol 31:298–301.

Levenspiel O. 1979. The chemical reactor omnibook. Corvallis, OR: OSU Book Stores.

Livansky K, Bartos J. 1986. Relationship between pCO_2 and pH in a medium for algal culture. Arch Hydrobiol Suppl 73:425–431.

Livansky K. 1982. Effect of suspension temperature on mass transfer coefficient of carbon dioxide from algal suspension into air on a cultivation platform with baffles. Arch Hydrobiol Suppl 63:363–367.

Livansky K. 1990. Losses of CO_2 in outdoor mass algal cultures: Determination of the mass transfer coefficient K_L by means of measured pH course in $NaHCO_3$ solution. Algological Studies 58:87–97.

Livansky K. 1992. Influence of some nutrient solution components and holding time of algal culture in CO_2 gas saturator on the allowable length of culture flow and other parameters of CO_2 supply into open cultivation units. Algological Studies 67:135–146.

Livansky K, Kajan M. 1993. pCO_2 and pO_2 profiles along the flow of algal suspension in solar culture units: Verification of a mathematical model. Algological Studies 70:97–119.

Livansky K, Prokes B. 1973, Some problems of CO_2 Absorption by algae suspensions. Biotechnol & Bioeng Symp 4:513–518.

Livansky K, Bartos J. 1987. Longitudinal profile of pCO_2 in algal suspension on an open-field cultivation surface. Arch Hydrobiol Suppl 73 (Algological Studies 45):587–598.

Markl H, Mather M. 1985. Mixing and aeration of shallow opend ponds. Arch Hydrobiol Beih 20:85–93.

Merchuk JC, Siegel MH. 1988. Airlift reactors in chemical and biological technology. J Chem Technol Biotechnol 41:105.

Molina Grima E, Sánchez Pérez JA, García Camacho F, Robles Medina A. 1993. Gas-liquid transfer of atmospheric CO_2 in microalgal cultures. J Chem Tech Biotechnol 56:329–337.

Molina Grima E, Chisti MY, Moo-Young M. 1997. Characterization of shear rates in airlift bioreactors for animal cell culture. J Biotechnol 54:195–210.

Molina Grima E, Fernández Sevilla JM, Sánchez Pérez JA, García Camacho F. 1996. A study on simultaneous photolimitation and photoinhibition in dense microalgal cultures taking into account incident and averaged irradiances. J Biotechnol 45:59–69.

Molina Grima E, García Camacho F, Sánchez Pérez JA, Urda Cardona J, Acién Fernández FG, Fernández Sevilla JM. 1994. Outdoor chemostat culture of Phaeodactylum tricornutum UTEX 640 in a tubular photobioreactor for the production of eicosapentaenoic acid. Biotechnol Appl Biochem 20:279–290.

Olaizola M, Duerr EO, Freeman DW. 1991. Effect of CO_2 enhancement in an outdoor algal production system using Tetraselmis. J Appl Phycol 3:363–366.

Pavlica RT, Olson JH. 1970.Unified design method for continuous-contact mass transfer operations. Ind Eng Chem 62(12):45–48.

Pirt SL, Lee YK, Walach MR, Pirt MW, Balyuzi HH, Bazin, MJ. 1983. A tubular bioreactor for photosynthetic production of biomass from carbon dioxide: Design and performance. J Chem Tech Biotechnol 33B:35–58.

Rados S, Vaclav B, Frantisek D. 1975. CO_2 Balance in industrial cultivation of algae. Arch Hydrobiol Suppl 46:297–310.

Richmond A, Boussiba S, Vonshak A, Kopel R. 1993. A new tubular reactor for mass production of microalgae outdoors. J Appl Phycol 5: 327–332.

Richmond A. 1991. Large scale microalgal culture and applications. In: Round FE and D.J. Chapman DJ, editor. Progress in phycological research. Bristol: Biopress Ltd., Bristol. vol 7. p 269–330.

Rotatore C, Colman B, Kuzma M. 1995. The active uptake of carbon dioxide by the marine diatoms Phaeodactylum tricornutum and Cyclotella sp. Plant Cell and Environ 18:913–918.

Talbot P, Gortares MP, Lencki RW, De la Noüe J. 1991. Absorption of CO_2 in algal mass culture systems: A different characterization approach. Biotechnol Bioeng 37:834–842.

Torzillo G, Pushparaj B, Bocci F, Balloni W, Materassi R, Florenzano G. 1986. Production of Spirullina biomass in closed photobioreactors. Biomass 11:61–64.

Torzillo G, Carlozzi P, Pushparaj B, Montaini E, Materassi R. 1993. A two plane tubular photobioreactor for outdoor culture of Spirulina Biotechnol Bioeng 42:891–898.

Tredici MR, Materassi R. 1992. From open ponds to alveolar panels: The Italian experience in the development of reactors for the mass cultivation of phototrophic microorganisms. J Appl Phycol 4:221–231.

Tsoglin LN, Gabel BV, Falkovich TN, Semenenko VE. 1996. Closed photobioreactors for microalgal cultivation. Rus J Plant Physiol 43: 131–136.

Weiland P, Oken U. 1981. Differences in the behavior of bubble columns and airlift loop reactors. Ger Chem Eng 4:174–181.

Weissman JC, Goebel RP, Benemann JR. 1988. Photobioreactor design: Mixing, carbon utilization, and oxygen accumulation. Biotechnol Bioeng 31:336–344.

Wenge F, Chisti MY, Moo-Young M. 1996. Slip–cylinder airlift reactors: Hydraulics and hydrodynamics of a new mode of operation. Chem Eng Commun 155:19–44.

Zuber N, Findlay JA. 1965. Average volumetric concentration in two phase flow systems. J Heat Transf Trans ASME 453–457.